# Simulate permeable reactive barrier by using a COMSOL model and comparison with the Thomas, Yoon–Nelson and Clark models for CR dye remediation by composite adsorbent (sewage and waterworks sludge)

Samara Saad Faraj, Rasha Salah Alkizwini and Maad F. Al Juboury

## ABSTRACT

The remediation of Congo Red (CR) dye by the synthetic sorbent composited from sewage and waterworks sludge was studied in batch and continuous experiments. The continuous experiments studied the composite synthetic after mixing with composite synthetic sorbent filter (CSF) glass waste to increase the hydraulic conductivity of the permeable reactive barrier (PRB). The synthetic composite sorbent was characterised by the nitrogen adsorption–desorption tests, field emission-scanning electron microscopy and X-ray diffraction. For evaluating the batch tests, the variable conditions of initial concentration, solution pH, agitation time and agitation speed were studied. The synthetic sorbent showed a high ability to remove the CR from a contaminated water, with maximum sorbent uptake equal to 9,469.211 mg/g and composite adsorbent-filter CSF equal to 4,415.946 mg/g. Pseudo-second-order kinetic model and Langmuir isotherm model governed the adsorption process. The column tests showed the highest reactivity, with 50:50 weight ratios of the adsorbent to filter glass waste. The experiments were done with different concentrations of CR and different bed heights of CSF as the PRB for 90 days. There was a delay in the breakthrough time when decreasing the contaminant concentrations and when increasing the composite adsorbent-filter CSF bed height. The breakthrough curves were well represented by the COMSOL model.

**Key words** | batch experiments, breakthrough curves, continuous system, glass waste, synthetic sorbent

**Samara Saad Faraj**
Environmental Science Department, Faculty of Science,
University of Zakho,
Zakho International Road, Zakho-Duhok, Kurdistan Region,
Iraq

**Rasha Salah Alkizwini**
Environmental Engineering department, Faculty of Engineering,
University of Babylon,
Babel,
Iraq

**Maad F. Al Juboury** (corresponding author)
Civil Engineering Department, Faculty of Engineering,
University of Kerbala,
Kerbala,
Iraq
E-mail: *maad.farooq@uokerbala.edu.iq*

## HIGHLIGHTS

- Remediation of the CR dye by the synthetic sorbent composited from sewage and waterworks sludge.
- This topic studies the use of the composite sorbent in the fixed bed column as a permeable reactive barrier.
- This study compares a COMSOL model with the Thomas, Yoon–Nelson and Clark models.

## INTRODUCTION

Internal and external sources contaminate groundwater. Internal sources originate inside or occur as a leachate when the groundwater flows through contaminated soils, while external sources result from leakages and spills (Hashim *et al.* 2011). Many agencies of contamination control and environmental protection have been trying to solve this global problem by applying technical and scientific resources with continuously high financial allocation. Membrane separation (Ciardelli *et al.* 2001), electrochemical technology (Shetti *et al.* 2019), constructed wetlands (Rahi

doi: 10.2166/wst.2020.500

et al. 2020), Pump-and-Treat systems (ITRC 2011; Sulaymon et al. 2015) and adsorption process (Faisal & Naji 2019; Abd Ali et al. 2020; Ahmed et al. 2020; Alshammari et al. 2020; Faisal et al. 2020a, 2020b, 2020c, 2020d; Naji et al. 2020) are considered developing technologies for treating water to remove several contaminants. Every process has advantages and disadvantages: for instance, the conventional Pump-and-Treat system gives good results initially, but over time gives bad results of treatment. Therefore, a good process with more advantages than disadvantages is the adsorption process (ITRC 2011; Sulaymon et al. 2015).

In order to protect the natural groundwater, and for remediation of many polluted areas, the permeable reactive barrier (PRB) as an element of the remedial integral programmes of groundwater in in-situ treatment have played a increasingly important role, which opens new horizons in the technology of remediation (Simon & Meggyes 2002). To prevent the restriction of the groundwater flow in the PRB, the reactive materials used in this technology, as its core element, must consist of large particles; and to prevent clogging, the particle size of these materials must be uniform. In addition, the reactivity of these materials must be maintained for a long duration; and to avoid secondary contamination of the groundwater, these materials must be non-hazardous. These reactive materials must be easily available and cost effective. Based on the difference of the treatment mechanisms and target pollutants, these materials have to be improved and used across a wide range (Ott 2000; Ambrosini 2004). It is important to satisfy the criteria of the filter design for the surrounding soil by choosing the grain size distribution, which is based on the geotechnical concentrations. Permeability, retention and internal stability criteria, which are the three main design criteria in one-dimensional flow conditions, must be met for the reactive media (Faisal et al. 2020c).

During long periods, the PRBs, which need minimum operational costs and maintenance, can be considered as a sustainable technology (Wantanaphong et al. 2005). The sustainability of PRB technology can be done using byproducts, recycled and waste materials such as maize cobs, non-living biomass, tree leaves, plant weeds and shells, paper ash, limestone dust, basalt dust, steel slag waste, blast furnace slag, activated sludge, steel fibres from tyres, shredded cast iron, recycled concrete, peat, fly ash and red mud (Faisal & Naji 2019; Abd Ali et al. 2020; Ahmed et al. 2020; Alshammari et al. 2020; Faisal et al. 2020a, 2020b, 2020c, 2020d; Naji et al. 2020).

EU legislation considers the waterworks sludge as 'non-hazardous' material. More than one million tonnes are produced annually, and in the future this quantity may increase. The surface water turbidity in the surrounding area of the sanitary landfills, into which the waterworks sludge is disposed of, can be increased by directly returning this sludge into the rivers in this area. In some countries an increase in the disposal process cost was recorded.

The soil can be improved by using sewage sludge as fertiliser because it contains organic substances such as nitrogen and phosphorus, which are produced by municipal wastewater treatment plants (WWTP) as a byproduct. A huge amount of sewage sludge may be dispersed into the ecosystem, for example that produced by the Al-Rostomia'a WWTP in Baghdad, Iraq. The problems resulting from disposal of the sewage and waterworks sludge can be minimised by using a cheaper solution by using different water companies (Basibuyuk & Kalat 2004).

In this study, the goal of reaching green projects and sustainable development was achieved by minimising the huge quantities of byproduct waste, and using them as sorbents for Congo Red dye (CR), which is considered a good solution for reducing the costs of disposal. Specifying the weight ratio for the composite synthetic sorbent filter (CSF) as the PRB, and characterising the remediation mechanism of the simulated wastewater contaminated with CR using a composite synthetic sorbent in batch experiments and CSF as the PRB in continuous experiments, optimised the results obtained for the theoretical and empirical models.

## MATERIALS AND METHODS

### Materials

The waste from Al-Rostomia'a WWTP in Baghdad was represented by the sewage sludge which was collected for reuse in the present study, after passing through several processes. It was washed with distilled water after drying under atmospheric temperature for 5 days. It was then crushed and sifted to obtain a particle 0.062–1 mm. At the end of the sludge preparation, the drying process was performed for 7 h at 80 °C (Doke et al. 2012; Simantiraki et al. 2013). The waterworks sludge from Al-Wehda WWTP, which is located in the same place as the previous WWTP, was used in this study. It contains aluminium because alum salts are used in the process of purifying. The waterworks sludge was air dried for 72 h and then crushed and sifted to obtain a particle with the same size as in the sewage sludge (Mathews & Zayas 1989). The element composition of the sewage

sludge and waterworks sludge is shown in section S1 (Supplementary Materials) and the pore size distribution of the sewage sludge and waterworks sludge = used in this study is shown in Table S2. The concentration of the CR was 1,000 mg/L, and it was kept under laboratory temperature (25 ± 2 °C). This dye was used to simulate the organic compounds that pollute an aqueous solution, and it was obtained from the Central Drug House (P) Ltd. To adjust the solution's pH, 0.10 mol/L of NaOH (or 0.1 mol/L of HCl) was added using successive dilutions to reach the required concentration for experiments.

## Preparation of composite sorbent

Alshammari *et al.*'s (2020) procedure was also used in this study to prepare the composite sorbent. A solution of 2 g $Fe(NO_3)_2$ equal to 50 mL of distilled water was used with the waterworks sludge and the sewage sludge at different percentages by adopting the method of modified precipitation. An orbital shaker was used for 180 min to stir this mixture to achieve the optimum percentage. A solution of $Fe(NO_3)_2$ at different concentrations was then used with a selected percentage of sludge, stirred by the orbital shaker for 180 min, and finally dried for 24 h at 105 °C to obtain particles which were stored for later use (Phuengprasop *et al.* 2011). The characterisation of sewage sludge, waterworks sludge and synthetic composite sorbent was carried out by X-ray diffraction (XRD) to examine the crystalline structures, and by field emission-scanning electron microscopy (FE-SEM) to examine the particle surface morphology.

## Sorption tests

The amount of CR dye solution equal to 100 mL and 0.01 g of sludge were added to all conical flasks from this mixture. Filter paper (type JJAO JIE 103) was used to filter the mixture to remove the solid particles from the solution. To measure the CR concentration, an analysis of filtered solution in a certain volume (≈10 mL) was performed on a UV/Vis spectrophotometer (Shimaze model: UV/VIS-1660) at the maximum wavelength of absorption of 498 nm. After a time period not exceeding 3 h samples were selected for use in the experiments according to the time of equilibrium. Additional tests at pH 2–13 were carried out to examine the effect on removal efficiency of the initial pH solution when the CR constant concentration was equal to 100 mg/L. The control temperature during the experiment was room temperature (25 ± 0.5 °C). The CR adsorption uptake ($q_e$) was obtained using Equation (1):

$$q_e = (C_o - C_e)\frac{V}{m} \quad (1)$$

where $V$ and $m$ are the amount of contaminated water (L) and the sorbent mass (g) in the flask respectively, and $C_e$ and $C_o$ are the equilibrium and initial CR concentrations.

## Continuous experiments

A Perspex column with the diameter and length equal to 250 mm and 50 cm, respectively, was used to set up the adsorbent in the present study as a continuous system of experiments. In addition, there were three sampling ports on the column at 10, 20 and 30 cm (port 1, port 2 and port 3, respectively) from the column base. These ports were blocked by a stainless steel Viton stopper on the column length. The syringe was used to take samples from the column's central axis through the ports at certain intervals. The CSF was packed in the total column length as a PRB, and the CR dye that simulated the contaminated groundwater filled the column by flowing into it through its base. The direction of flow rate was upward from a storage tank using two valves and a flow meter (Figure 1). The discharge rate of the contaminated water for the continuous experiments was 30 mL/min and the initial concentration of the contaminant in this water was 500, 1,000 and 1,500 mg/L. The sampling was done periodically every 5 days for 90 days. The concentration of the contaminant and the discharge rate of the contaminated water passing into the bed were constant during the experiments. All materials used for the lines of effluent and influent of

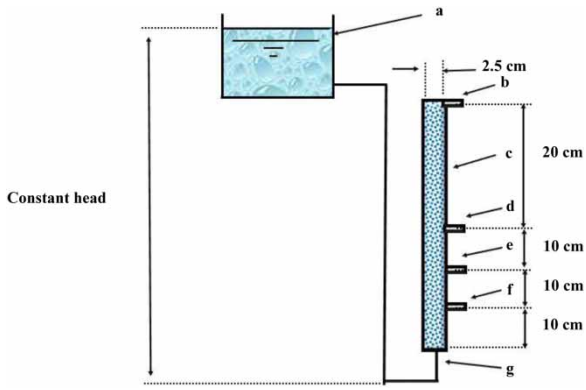


**Figure 1** | Schematic diagram of the laboratory-scale bed: (a) storage tank, (b) outflow, (c) perspex column, (d) port 3, (e) port 2, (f) port 1, (g) inflow.

the continuous system were inert materials, including fitting and tubing. The benefit of using continuous system experiments is to facilitate the design of a field-scale PRB with a good simulation by modelling and characterising these experiments.

It is important to note that when comparing the hydraulic conductivity for the composite adsorbent with that for other reactive media, it was found to be lower. This property has negative effects, especially in the column experiments, because it leads to clogging the bed (sorbent material) and stopping the water from flowing through it. Therefore, the adsorbent should be mixed with coarse materials such as tyre chips, coarse sand or gravel to increase the hydraulic conductivity (Mishra *et al.* 2011). Based on the principle of environmental preservation of waste and reuse, the glass waste was collected, washed, crushed and sieved (0.35 mm), then it was used as the inert filler material by mixing it with modified adsorbent to increase the hydraulic conductivity value, which prevents a blockage of the bed. Two tested reactive systems were used in the column experiments by mixing the adsorbent with glass waste. This system was a 1:1 mixture of adsorbent and glass waste.

## RESULTS AND DISCUSSION

### Characterisation of different materials

#### FE-SEM images and XRD analysis

The sewage sludge, waterworks sludge and the composite sorbent were characterised by XRD analysis, and their crystalline structures can be seen in Figure 2(a), 2(d) and 2(g). This figure shows the sewage sludge composition recognised by the iron oxide and the hydroxyapatite. It also shows that the waterworks sludge's main components are iron oxide, calcite and silica oxide.

The sewage sludge, waterworks sludge and the composite sorbent were also characterised by FE-SEM images and surface morphology (Figure 2(b), 2(e) and 2(h)). The smoothly compacted pore structure and the construction of a plate-like layer in the sewage sludge are shown in Figure 2. The FE-SEM images for this sludge consist of roughly aggregated micrometric plates (with high surface/volume ratio) with irregular orientations and size (Amaniampong *et al.* 2018, 2015). The adsorbent efficiency can be enhanced by the high exposed surface area for the adsorption process. In addition, the enhancing microstructure presented by the block, dense and intact structure of the waterworks sludge is shown in Figure 2(b), 2(e) and 2(h), while the FE-SEM images of composite adsorbent (Figure 2(b), 2(e) and 2(h)) show more edge due to the reaction of iron nitrate with the sludge.

#### The test of adsorption–desorption for the nitrogen

The isotherms of the adsorption–desorption nitrogen for sewage sludge, waterworks sludge and composite adsorbent are presented in Figure 2(c), 2(f) and 2(i). These isotherms were of type-II with deBoer hysteresis loops. A slow rising trend of adsorption isotherm at relative pressure ($P/P_0$) > 0.47 and obvious lag phenomenon of desorption isotherm were attributed to the capillary condensation and multilayer adsorption. The results of nitrogen adsorption–desorption isotherms suggested massive mesoporosity in the structure of the adsorbent (Hu *et al.* 2018). The type of inter-aggregated pores can be specified from the pressure of the hysteresis loop. It is larger, producing intra-aggregated secondary particles, and also finer, resulting in inter-agglomerated primary particles when the pressure is in the range $0.8 < P/P_0 < 1$ and in the range $0.4 < P/P_0$, respectively.

#### Influences of batch conditions

The removal efficiency of CR dye, effected by an agitation speed with a range of 0–250 rpm, is evident in Figure 3(a), and other parameters for the experiment (time = 3 h, pH = 3, $C_o$ = 100 mg/L and dose = 0.01 g/100 mL) were kept constant. When the agitation speed was equal to zero (before shaking), the sorption uptake of the contaminant was 420 mg/L, and it gradually increased as the rate of shaking increased, reaching 960 mg/g at an agitation speed equal to 200 rpm, which is considered the best equilibrium. This increase can be explained as the diffusion of CR in the direction of the adsorbent surface, which may be improved when increasing the agitation speed. All the adsorbent sites became easily available for adsorption of the pollutant at 200 rpm, which gave a higher adsorption capacity (Jin *et al.* 2014; Faisal & Naji 2019; Faisal *et al.* 2020b; Naji *et al.* 2020).

Figure 3(b) shows the pH effect on the adsorption of CR from contaminated solution at pH 3–13, when the other parameters for the experiment (time = 3 h, agitation speed = 200 rpm, $C_o$ = 100 mg/L and dose = 0.01 g/100 mL) were kept constant. A pH of 3.1 was used in the experiment as the lowest value, because pH <2 decreases the dye solubility. When pH <5, the colour of the dye was dark blue and when pH ≥7 the colour was red (Sahoo *et al.* 2019).

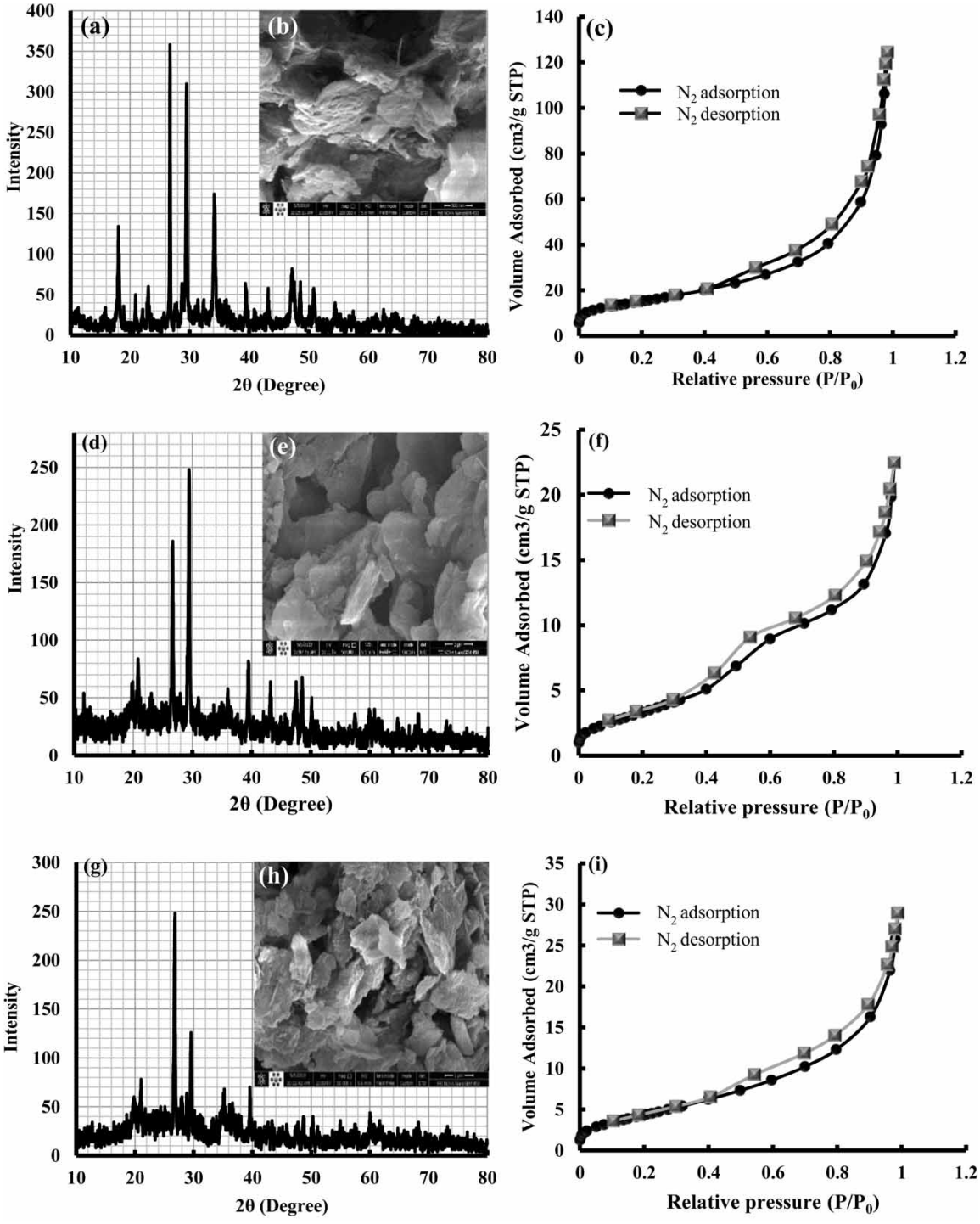


**Figure 2** | The characterisation of (a, d, g) XRD, (b, e, h) FE-SEM and (c, f, i) $N_2$ adsorption–desorption curve patterns of (a, b, c) waterworks, (d, e, f) sewage sludge and (g, h, i) composite adsorbent.

At a pH value ranging from 3.1 to 6, the CR dye removal efficiency was 96%. This removal efficiency decreased when increasing the pH, becoming 17% at pH 13. Therefore, 96% was considered the maximum removal efficiency. The gradual decrease of removal efficiency may be from the competition of the anionic contaminant with the increasing

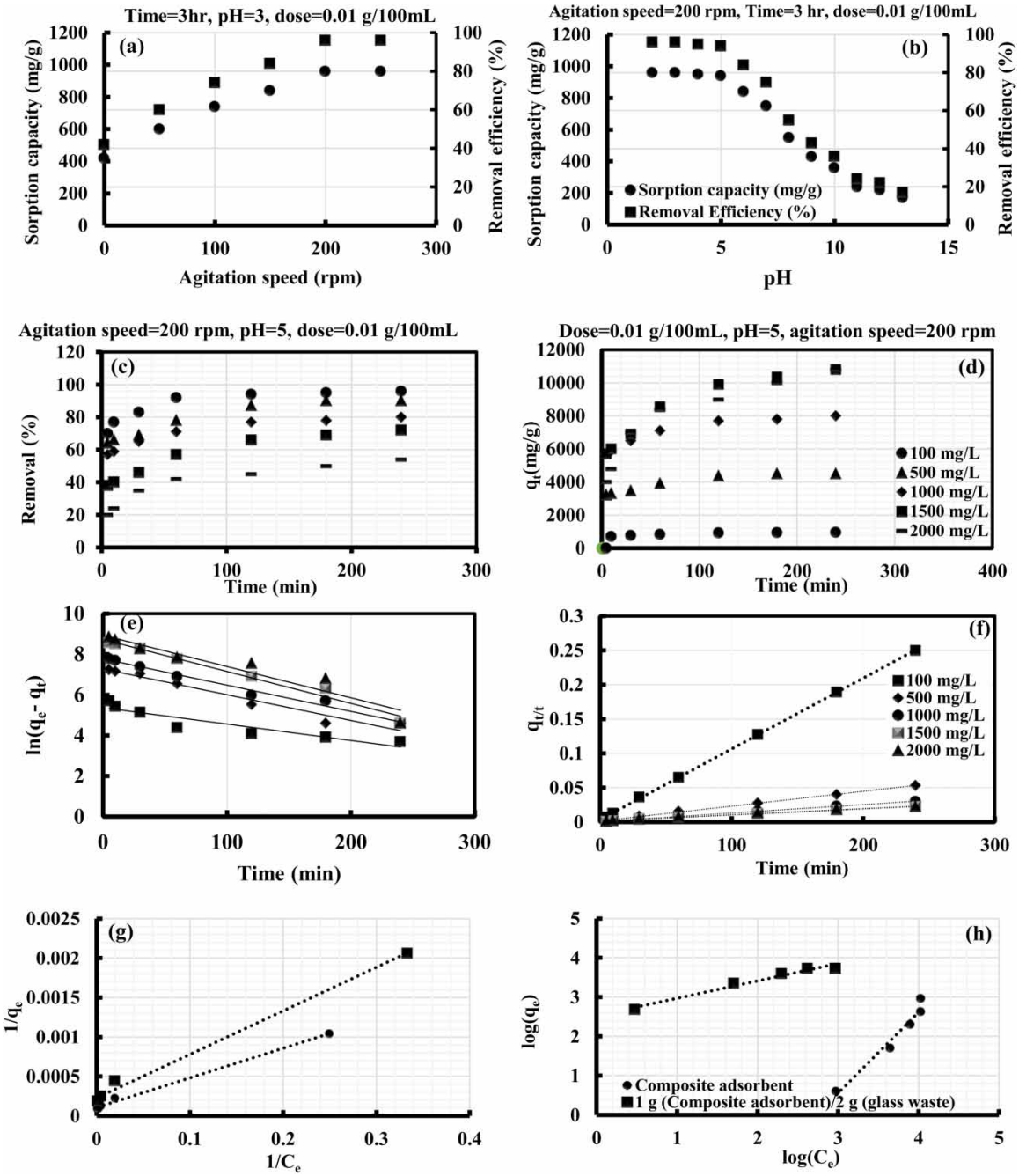


**Figure 3** | The effect of (a) agitation speed, (b) pH, (c) initial concentration and contact time, (d) sorption capacity of contact time. Initial concentration experiment represented the kinetic models (e) pseudo-first-order and (f) pseudo-second-order; and the isotherm models: (g) Langmuir and (h) Freundlich.

amount of hydroxide ion ($OH^-$) on the adsorbent surface, and also from the electrostatic repulsion between the surface sites' negative charges and anionic contaminant. However, there was a strong electrostatic attraction at pH = 3 between the surface sorbent positive charge and the anionic dye, which explains the higher removal efficiency at this pH. The adsorption of CR dye on amine-functionalised magnetic iron oxide nanoparticles (Sahoo *et al.* 2019) gave the same results. It obvious from the XRD that the CR removal has a very good adsorptive affinity due to the iron oxides in the adsorbent, which interact with amine ($NH_2$) and sulfonate ($SO_3$) groups in the structure of CR (Singuru *et al.* 2016; Sarkar *et al.* 2019). The second interactive mode between the synthetic sorbent

and the CR molecules are represented by the strong coordination between the aromatic rings in CR with the surface of metal and metal oxides. This interaction may also allow the synthetic adsorbent for adsorption of CR dye (Paul *et al.* 2020; Sarkar *et al.* 2020). This interaction may also allow the synthetic adsorbent to adsorb CR dye.

The adsorption of CR from contaminated water on the adsorbent was affected by the initial concentrations of the contaminant and so this effect was studied at different concentrations (100, 500, 1,000, 1,500 and 2,000 mg/L) and with other constant parameters (pH = 3, agitation speed = 200 rpm and dose = 0.01 g/100 mL) (Figure 3(c)). It is obvious from this figure that when the initial CR concentration was high, there was a slight increase of contaminant at equilibrium sorbed on the sorbent and when the concentration was low, there was a rapid increase of the pollutant adsorbed on the composite sorbent. This means that higher removal efficiency was at lower CR initial concentrations, and this decreased when the concentration increased. The decrease in removal efficiency is because when the concentrations of the contaminants increase, the favourable sites become fewer, due to the available active sites becoming saturated (Buasri *et al.* 2008). Figure 3(c) also shows the contact time effect on the removal efficiency of CR at different initial concentrations. Within 1 h, the sorption equilibrium was established, and this time was selected for all tests to reach the time of equilibrium.

There are two stages of the adsorption process, as can be seen in Figure 3(d). They are rapid and slow adsorption, which occur in the initial and subsequent adsorption, respectively. When comparing the adsorption capacity of the second with the first stage, it increased much more slowly, until it did not vary significantly at the end. This phenomenon can be explained by the mass transfer processes: the CR quickly touches the adsorbent surface boundary layer at the initial time of adsorption. After that, the contaminant is diffused slowly from the boundary layer because it occupies some of the many available external sites, which are diffused to the adsorbent porous structure (Faisal *et al.* 2020a; Naji *et al.* 2020).

## Sorption data kinetic models

### Pseudo-first-order model

Equation (2) represents the expression of this model, describing the adsorption rate of CR from contaminated solution. The expression in Equation (2) produces Equation (3) when $q_t = q_e$ at time $t$ and $q_t = 0$ at $t = 0$ (Lagergren 1989):

$$\frac{dq}{dt} = k_1(q_e - q_t) \tag{2}$$

$$\ln(q_e - q_t) = \ln q_e - k_1 t \tag{3}$$

### Pseudo-second-order model

This model is written in Equation (4), with an assumption that no interaction between the contaminants can occur, the sorption energy for every reactive material remains the same, and a monolayer formed between the sorbate and the sorbent. The expression in this equation produces Equation (5) when applying the same conditions previously mentioned in the first-order model (Ho & McKay 1999):

$$\frac{dq}{dt} = k_2(q_e - q_t)^2 \tag{4}$$

$$\frac{1}{(q_e - q_t)} = \frac{1}{q_e} + k_2 t \tag{5}$$

where the pseudo-first-order rate constant is $k_1$ (1/min) and the pseudo-second-order rate constant is $k_2$ (g/mg min).

The adsorption kinetics studies were conducted for examining the adsorption rate and the mechanism. The tests were done with the following constants: pH = 3, agitation speed = 200 rpm and dose = 0.01 g/100 mL, and at different values of contact times and CR concentrations. Table 1 and Figure 3(e) and 3(f) show the results for experiments of the kinetic models, and it is obvious from this figure that the adsorption process (based on higher $R^2$) has is better represented by the pseudo-second-order than the first-order kinetic model (Sepehr *et al.* 2014).

## Sorption isotherms

The curve resulting from plotting the remaining CR equilibrium concentration in the contaminated solution ($C_e$ by mg/L) versus the CR dye amount per composite adsorbent unit weight ($q_e$ by mg/g) represented the isotherm that describes the adsorption process (Limousin *et al.* 2007). This curve, when the concentration in the fluid is proportional to the amount adsorbed, goes through the origin, giving the linear isotherm. The upward concaving curve leads to relatively high mass transfer area and to low solid loading of contaminant, and so it gives an unfavourable isotherm. The upward convexity curve

**Table 1** | An initial concentration experiment representing the kinetic models pseudo-first- and second-order

| Initial concentration | Model | Constant | Composite adsorbent |
|---|---|---|---|
| 100 mg/L | Pseudo-first-order | $k_1$ | 0.0081 |
| | | $q_e$ | 214.0857 |
| | | $R^2$ | 0.8490 |
| | Pseudo-second-order | $q_e$ | 969.8324 |
| | | $k_2$ | 0.0003 |
| | | $R^2$ | 0.9999 |
| 500 mg/L | Pseudo-first-order | $k_1$ | 0.0127 |
| | | $q_e$ | 1,445.0902 |
| | | $R^2$ | 0.9558 |
| | Pseudo-second-order | $q_e$ | 4,613.9259 |
| | | $k_2$ | 0.0000 |
| | | $R^2$ | 0.9987 |
| 1,000 mg/L | Pseudo-first-order | $k_1$ | 0.0129 |
| | | $q_e$ | 2,377.0914 |
| | | $R^2$ | 0.9834 |
| | Pseudo-second-order | $q_e$ | 8,099.1535 |
| | | $k_2$ | 0.00002289 |
| | | $R^2$ | 0.9993 |
| 1,500 mg/L | Pseudo-first-order | $k_1$ | 0.0157 |
| | | $q_e$ | 6,165.8898 |
| | | $R^2$ | 0.9752 |
| | Pseudo-second-order | $q_e$ | 11,163.9532 |
| | | $k_2$ | 0.000007 |
| | | $R^2$ | 0.9965 |
| 2,000 mg/L | Pseudo-first-order | $k_1$ | 0.0154 |
| | | $q_e$ | 7,571.5303 |
| | | $R^2$ | 0.9139 |
| | Pseudo-second-order | $q_e$ | 11,113.0124 |
| | | $k_2$ | 0.000006 |
| | | $R^2$ | 0.9936 |

leads to obtaining more solid contaminant from the solution at low concentration, thus giving a favourable isotherm. According to these types, and basing on the system of the contaminant–adsorbent, the sorption process is a specific property. An irreversible adsorption results from a favourable limiting case, where the contaminant amount does not depend on concentrations at lower values (Limousin *et al.* 2007). In this study, two isotherm models were used: the Freundlich and the Langmuir. The first is the adsorption to surfaces supported by different affinity sites or to heterogeneous surfaces, and is empirical in nature. The assumption of this isotherm is that when the site occupation degree is increased, the binding strength is decreased, and the initial occupation is to the stronger binding sites. This isotherm can be quantified by Equation (6), while Equation (7) represents its linear form expression (Miz *et al.* 2014; Saad *et al.* 2019; Ahmed *et al.* 2020).

$$q_e = K_F C_e^{\frac{1}{N}} \quad N > 1 \tag{6}$$

$$\log q_e = \log K_F + \frac{1}{N}\log C_e \tag{7}$$

The adsorption intensity is indicated by empirical coefficient $N$ and the Freundlich sorption is represented by the coefficient $K_F$ (mg/g)(L/mg)$^{1/N}$.

The second model can be expressed by Equation (8) and the linear form expression of the second model (Equation (8)) is shown in Equation (9). It is assumed that the contaminant is not transmigrated in the surface plane, the sorption energy is fixed and the higher sorption of the contaminant has corresponded to a single-layer sorption on the surface sorbent (Naji *et al.* 2019).

$$q_e = \frac{q_m b C_e}{1 + bC_e} \tag{8}$$

$$\frac{C_e}{q_e} = \frac{1}{q_m b} + \frac{1}{q_m} C_e \tag{9}$$

The maximum adsorption capacity is represented by $q_m$ and the adsorption free energy constant is represented by $b$.

Accordingly, from the linear plotting (value of the intercept and the slope), the empirical coefficients (Table 2) for each model were calculated (Figure 3(g) and 3(h)) using Microsoft Excel 2010 software. The Langmuir model is better at representing the CR dye adsorption process than the other isotherm models, as shown in Table 2 and Figure 3(g) and 3(h). The transporting of a pollutant from the solution to the PRB adsorbent in the column system can be governed by the equation of partial differential, which can describe the CR dye adsorption by using the good fit isotherm model in this equation.

## Influence of various parameters of continuous system experiments on contaminant sorption

The constant adsorbent mass can treat the smaller volume of inflow solution with a highly concentrated inflow solution (Markovska *et al.* 2001). A constant dye amount in the inflow solution can be adsorbed by a given adsorbent mass, and so it is important to examine the contaminant concentration effect as a main process parameter and a limiting factor. The different initial concentrations of CR (500, 1,000 and 1,500 mg/L) were used in the continuous system experiments when fixing the value of flow rate to

**Table 2** | The isotherm models for CR dye sorption by composite adsorbent and CSF

| Model | | Composite adsorbent | CSF |
|---|---|---|---|
| Langmuir | $R^2$ | 0.9962 | 0.9933 |
| | Intercept | 0.0001 | 0.0002 |
| | Slope | 0.0037 | 0.0055 |
| | $q_{max}$ | 9,469.211 | 4,415.9460 |
| | $b$ | 0.0281 | 0.0409 |
| Freundlich | $R^2$ | 0.9585 | 0.9689 |
| | Intercept | 2.7726 | 2.5285 |
| | Slope | 0.4654 | 0.4425 |
| | $N$ | 2.1485 | 2.2596 |
| | $K_F$ | 592.3911 | 337.6924 |

30 mL/min and different bed heights: 10 cm (port 1), 20 cm (port 2), and 30 cm (port 3). It is obvious from the Figure 4 that the breakthrough was flat, late occurring and after a long duration. The adsorbent saturation occurred when using low initial concentrations of the contaminant as the process was controlled by the film, and the mass transfer zone was wide. However, when the breakthrough was sharp, quickly occurring and after a short duration, the adsorbent saturation occurred when using high initial concentrations of the contaminant, as the process was controlled by the mass transfer zone (was small) and intraparticle diffusion. Other researchers have reported similar results (Hadi *et al.* 2011; Bharathi & Ramesh 2013; Somasekhara & Nirmala 2019). According to these results, the breakthrough time and the saturation are affected by the change of initial concentration of contaminant (Goel *et al.* 2005). When the concentration is low, the diffusion coefficient is decreased and the transport is slower, which gives a higher treated volume and a delayed adsorbent (Padmesh *et al.* 2005; Han *et al.* 2007).

As mentioned above, different bed heights (10 cm–port 1, 20 cm–port 2 and 30 cm–port 3) of the adsorbents were used to examine the adsorbent mass effect on the sorption process, with a fixing value of flow rate equal to 30 mL/min of the solution contaminated with different concentrations of CR passing through the bed (Figure 4). The effect of this parameter was studied because the total mass of the sorbent is considered a strong function of the bed height, and the sorbent quantity is limited to the contaminant accumulation in the bed (Mobasherpour *et al.* 2014). Figure 4 shows that an increase in the bed height leads to an increase in the breakthrough time. This means that the variation of the bed height has a positive relationship with the exhaustion time, the breakthrough time, the treated solution volume, the sorption efficiency and the bed capacity (Al-Degs *et al.* 2009; Saha *et al.* 2012; Mobasherpour *et al.* 2014). The explanation of this phenomenon is that the increase in the adsorbent mass leads to an increase in the diffusion of the contaminant molecules to the sorbent due to a decrease in the axial dispersion of the mass transfer. High effluent volume can therefore be treated because the solution stays in the bed for enough time to diffuse the sorbent (Li *et al.* 2011). Several researchers have reported similar results (Mobasherpour *et al.* 2014; Sadaf & Bhatti 2014).

### Recyclability

During the sorption process, the performance stability and regeneration capacity of the adsorbent mainly control the practical application. The regeneration of the exhausted adsorbent and the removal of the CR dye molecules are done by using the adsorbent in NaOH solution with a concentration of 0.1 mol/L for 3 h. This process represents the recyclability tests for the adsorbent in this study. Reusing the adsorbent for the adsorption of CR dye gave a high removal efficiency of more than 90%. Section S3 (Supplementary Materials) shows the results of the reused adsorbent after seven rounds of recycling. For the treatment of contaminated water with anionic dye, the composite adsorbent is a promising adsorbent, as the results indicated.

### The coefficient of longitudinal dispersion

The longitudinal dispersion coefficient ($D_L$) measurement with a variation of velocity ($V$) can be dealt with using the experimental results for CSF, and Equation (10) is used to describe it. Equation (11) is consistent with the form's general expression of $D_L$.

$$D_L = 7.7921V + 0.5088 \quad R^2 = 0.9683 \tag{10}$$

$$D_L = D_{\text{mech}} + D^* \tag{11}$$

The coefficient of the effective molecular diffusion and of the mechanical dispersion are represented by $D^*$ and $D_{\text{mech}}$, respectively.

## Application of the theoretical models

### COMSOL model

Equation (12) describes the advection–dispersion transport of one-dimensional solution in the saturated zone of soil. As discussed above, the Langmuir sorption isotherm governs the adsorption process of the CR from contaminated

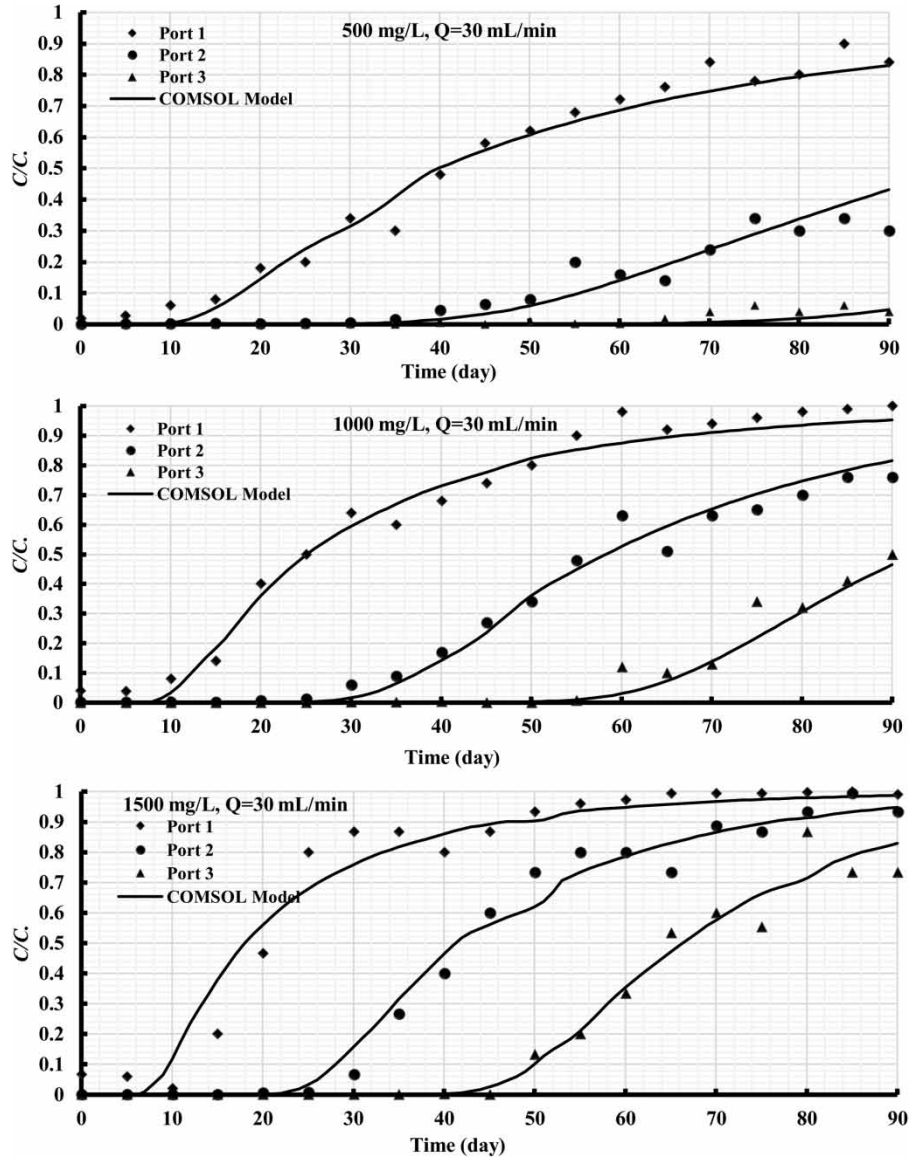


**Figure 4** | Breakthrough curves and COMSOL model with a different initial concentration of the CR dye and different mass adsorbent.

water on the adsorbent-filter glass waste, and Equation (13) expresses the retardation factor.

$$D_z \frac{\partial^2 C}{\partial z^2} - V_z \frac{\partial C}{\partial z} = R \frac{\partial C}{\partial t} \tag{12}$$

$$R = 1 + \frac{\rho_b}{n}\left(\frac{4415.946174 \times 0.040994498}{(1 + 0.040994498C)^2}\right) \tag{13}$$

The pollutant type transport relative to the advection frontal is retarded by the factor of retardation $R$ (assuming that the $R$ for contaminant transport in the column was equal to one). The CR dye concentration was represented by $C$, the flow velocity was represented by $V_z$ and the coefficient of dispersion in the $z$ direction was represented by $D_z$, the sorbent-filter glass waste porosity was represented by $n$, the concentration (mg/L) of the solution was represented by $C$ and the bulk density (g/cm$^3$) was represented by $\rho_b$.

The previous equation can be used to present the theoretical verification for the bed experiment in the range $0 \leq z \leq 50$ cm by using the sorbent-filter glass waste as PRB. By considering the method of finite element to be the base for the COMSOL Multiphysics 3.5a software, the COMSOL model was applied using the parameters: aquifer

porosity ($n_A$) 0.43, longitudinal dispersivity ($\alpha_L$, cm) 7.7921 and $\rho_b$ (g/cm$^3$) 1.0365 (Figure 4). The predicted concentrations of the initial concentrations, solved numerically, after passing through the packed bed from the sorbent, showed that the PRB adsorbed the pollutants and the concentration level of the solution in the outflow reached around zero. Figure 4 shows that the experimental results with the predicted COMSOL fit best with $R^2$ equal to 0.96.

## Thomas model

Different researchers use the simple Thomas model (Equation (14)), and the mass conservation equation was derived from this model in a continuous system (Thomas & Crittenden 1998). The Thomas model assumptions are that the Langmuir model controls the sorption process with an absence of axial dispersion, and that the second-order kinetics are the driving force for the adsorption process (Padmesh *et al.* 2005).

$$\ln\left(\frac{C}{C_0}-1\right)=\frac{(Mq_0k_{Th})}{Q}-\frac{K_{Th}C_0t}{1000} \tag{14}$$

The maximum sorption capacity (mg/g) was represented by $q_o$, the constant of the Thomas rate (L/min g) was represented by $K_{Th}$, the contaminant concentration in the influent (mg/L) in the contaminated water was represented by $C_o$, the adsorbent mass was represented by $M$, the flow rate was represented by $Q$ and the time was represented by $t$.

By using Microsoft Excel 2016 with linear fitting of breakthrough curve experimental data with Equation (14), the parameters $q_o$ and $K_{Th}$ of the model can be estimated. The Thomas kinetic model was used to determine the constant of the sorption rate $K_{Th}$ and the $q_o$ of the CR, using the data obtained in the bed system experiments from the linear results (values of intercepts and slope) from the plotting of ln[($C_o$/$C$) – 1] versus time. Figure 5 shows the estimated value obtained by applying the Thomas model to a different mass of the sorbent in the bed and to different CR concentrations in the inflow solution. Table 3 shows that the values of $q_o$ increased and $K_{Th}$ decreased for the experimental and Thomas model theoretical parameters when the concentration of the CR was increased. The explanation for this is that when the concentration of CR is higher, the column performance is better due to a higher driving force, as this force is equal to the difference between the pollutant concentration on the sorbent and the pollutant concentration in the contaminated water (Han *et al.* 2007). Also, with an increase in the height of the bed (adsorbent mass), the value of $K_{Th}$ was increased, and the value of $q_o$ was decreased. The CR dye adsorption therefore increased when the adsorbent bed height was higher and when the concentration of CR dye was lower. For different systems, similar forms of $K_{Th}$ were reported by Bharathi & Ramesh (2013) and Yagub *et al.* (2015). Depending on the value of $R^2$, the Thomas model was a better fit with the experimental value, which indicates that the limiting step is not the diffusion (internal and external) (Baral *et al.* 2009).

## Yoon–Nelson model

It is not important to know the detailed data related to the physical properties of the sorption column, the sorbent type and the adsorbate characteristics when using the less complicated Yoon–Nelson bed model (Equation (15)) (Yagub *et al.* 2015). The possibility of adsorbate breakthrough and adsorption on the sorbent being proportional to the rate of reduction and the possibility of every adsorbate molecule adsorption and is the base for the model assumption (Bharathi & Ramesh 2013).

$$\ln\left(\frac{C}{C_0-C}\right)=K_{\mathrm{YN}}t-K_{\mathrm{YN}}\tau \tag{15}$$

The time (min) for 0.5% of CR dye breakthrough was represented by $\tau$, the time (min) for breakthrough (sampling) was represented by $t$, the concentration of the outflow (mg/L) was represented by $C$, the concentration of the inflow (mg/L) was represented by $C_o$ and the Yoon–Nelson constant (min$^{-1}$) was represented by $K_{\mathrm{YN}}$.

The straight line with intercept $K_{\mathrm{YN}}\tau$ and slope of $K_{\mathrm{YN}}$ resulted from the application of Equation (15) to obtain bed data from adsorbate adsorption at different bed depths (100, 200 and 300 mm) and different initial pollutant concentrations (500, 1,000 and 1,500 mg/L), with the plotting of $\ln\left(\frac{C}{C_0-C}\right)$ against $t$ (Figure 6). From this, we can calculate the values of the parameters ($\tau$ and $K_{\mathrm{YN}}$) and perform the linear regression (Table 3). It is clear in this table that the values of $K_{\mathrm{YN}}$ decreased and the value of $\tau$ increased when the bed heights increased. At higher inflow concentration, this model was an effective simulation of the whole adsorbent because the uptake rate can increase when the competition between contaminant molecules for the sorption site increases, as the initial concentration of the adsorbate was increased (Hamdaoui 2006). CR dye adsorption by melon peel was reported with a similar

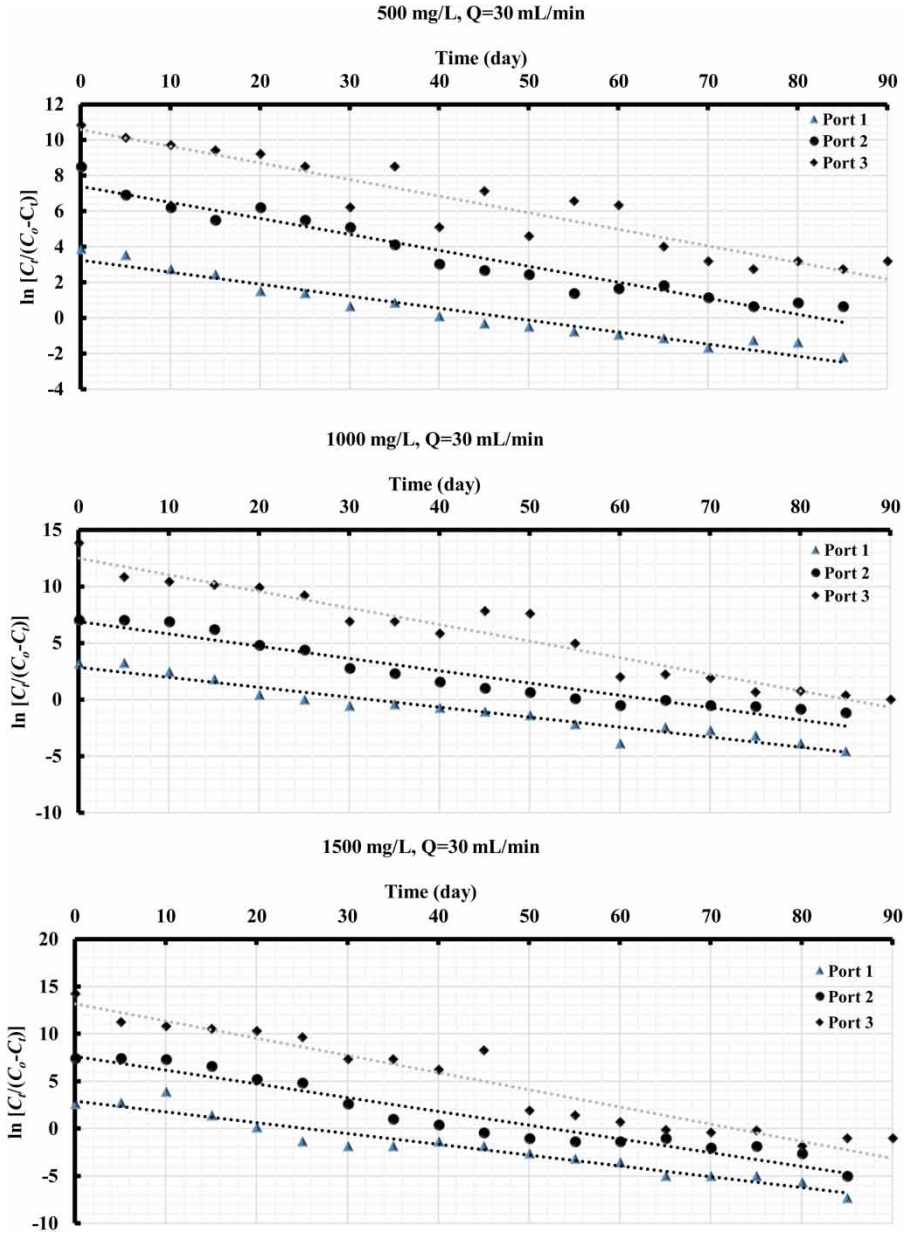


**Figure 5** | Thomas model of breakthrough curves for CR with 30 mL/min flow rate and different initial concentration on adsorption.

trend (Djelloul & Hamdaoui 2014). The value of $R^2$ equal to 0.92 (Figure 6 and Table 3) indicated that the Yoon–Nelson model was suitable for this suggested column and had a good fit with the experimental data.

## Clark model

The assumption of the Clark model is that the type of flow is a piston, that the Freundlich isotherm controls the contaminant adsorption process, and the development of the kinetic equation gives the linearised form of the Clark model (Equation (16)) (Clark 1987).

$$\ln\left[\left(\frac{C}{C_0}\right)^{n-1} - 1\right] = \ln A - e^{-rt} \tag{16}$$

The Freundlich isotherm exponent corresponded to $n$ and the kinetic model parameters were represented by $A$ and $r$.

**Table 3** | The parameters of the Thomas, Yoon–Nelson and Clark models

| Model | Initial concentration (mg/L) | Parameter | Port 1 | Port 2 | Port 3 |
|---|---|---|---|---|---|
| Thomas model | 500 | $K_{Th}$ | 0.134853 | 33.36544 | 197.5413 |
| | | $q_o$ | 15.70133 | 0.050051 | 0.008067 |
| | | $R^2$ | 0.946234 | 0.940969 | 0.889387 |
| Yoon–Nelson model | | $K_{YN}$ | 0.063769 | 0.111536 | 0.093995 |
| | | $\tau$ | 49.37206 | 65.09904 | 105.3873 |
| | | $R^2$ | 0.932284 | 0.927685 | 0.889839 |
| Clark model | | $A$ | 50.82422 | 8955.138 | 611173.8 |
| | | $r$ | 0.071359 | 0.104180 | 0.117054 |
| | | $R^2$ | 0.918935 | 0.922941 | 0.889122 |
| Thomas model | 1,000 | $K_{Th}$ | 0.088031 | 9.315556 | 20.25710 |
| | | $q_o$ | 22.04926 | 0.171727 | 0.081607 |
| | | $R^2$ | 0.942228 | 0.929143 | 0.937327 |
| Yoon–Nelson model | | $K_{YN}$ | 0.088031 | 0.152609 | 0.146423 |
| | | $\tau$ | 32.37591 | 44.16187 | 85.31570 |
| | | $R^2$ | 0.942228 | 0.919422 | 0.937327 |
| Clark model | | $A$ | 33.40020 | 4372.796 | 6339098 |
| | | $r$ | 0.094662 | 0.122512 | 0.181262 |
| | | $R^2$ | 0.933765 | 0.906970 | 0.935718 |
| Thomas model | 1,500 | $K^{Th}$ | 0.076082 | 6.515967 | 9.789385 |
| | | $q_o$ | 26.94492 | 0.287580 | 0.184112 |
| | | $R^2$ | 0.933928 | 0.931910 | 0.930167 |
| Yoon–Nelson model | | $K_{YN}$ | 0.114123 | 0.198001 | 0.172539 |
| | | $\tau$ | 25.44973 | 37.21973 | 77.52051 |
| | | $R^2$ | 0.933928 | 0.913729 | 0.920647 |
| Clark model | | $A$ | 34.47409 | 8737.243 | 13711869 |
| | | $r$ | 0.120568 | 0.157593 | 0.221106 |
| | | $R^2$ | 0.921252 | 0.901311 | 0.926143 |

The dynamic adsorption is described by the particularly attractive approach of the Clark model, and the rate constants of this adsorption can be determined by the precise analytical solution of the Clark model. When comparing the Freundlich sorption isotherms with this model, the second theory is based on the concept of a mass transfer (Aksu & Gönen 2004). By utilising the analysis of a linear regressive, the parameters of this model ($r$ and $A$) can be calculated from the plotting of $\ln\left[\left(\frac{C}{C_0}\right)^{n-1} - 1\right]$ against time (Figure 7 and Table 3) and then used in Equation (16) to determine the concentration of the Clark model. From this result, the Clark model had a low adsorption breakthrough.

## CONCLUSIONS

The synthesis of composite sorbent from byproduct wastes (sewage and waterworks sludge) is the innovation of the present study. When used for adsorption of CR it showed a good ability to remediate simulated contaminated water. XRD, FE-SEM and nitrogen adsorption–desorption tests were used to characterise this composite sorbent. The variable conditions of initial concentration, solution pH, agitation time and agitation speed were studied to evaluate the batch tests. The adsorption of CR, with a maximum adsorption capacity reaching 9,469.211 mg/g, was good and followed the Langmuir isotherm with $R^2$ not less than 0.99. It was also a good fit with the pseudo-second-order kinetic model. The CSF glass waste with a 50:50 weight ratio was used as the PRB in the bed system, and the experiments were done with different initial concentrations of dye and different mass of adsorbent to study their effect on the adsorption process. The results showed that higher adsorption capacity was achieved when the initial dye was increased, and the sorption performance improved when the bed height was increased. When the concentration was low, the diffusion

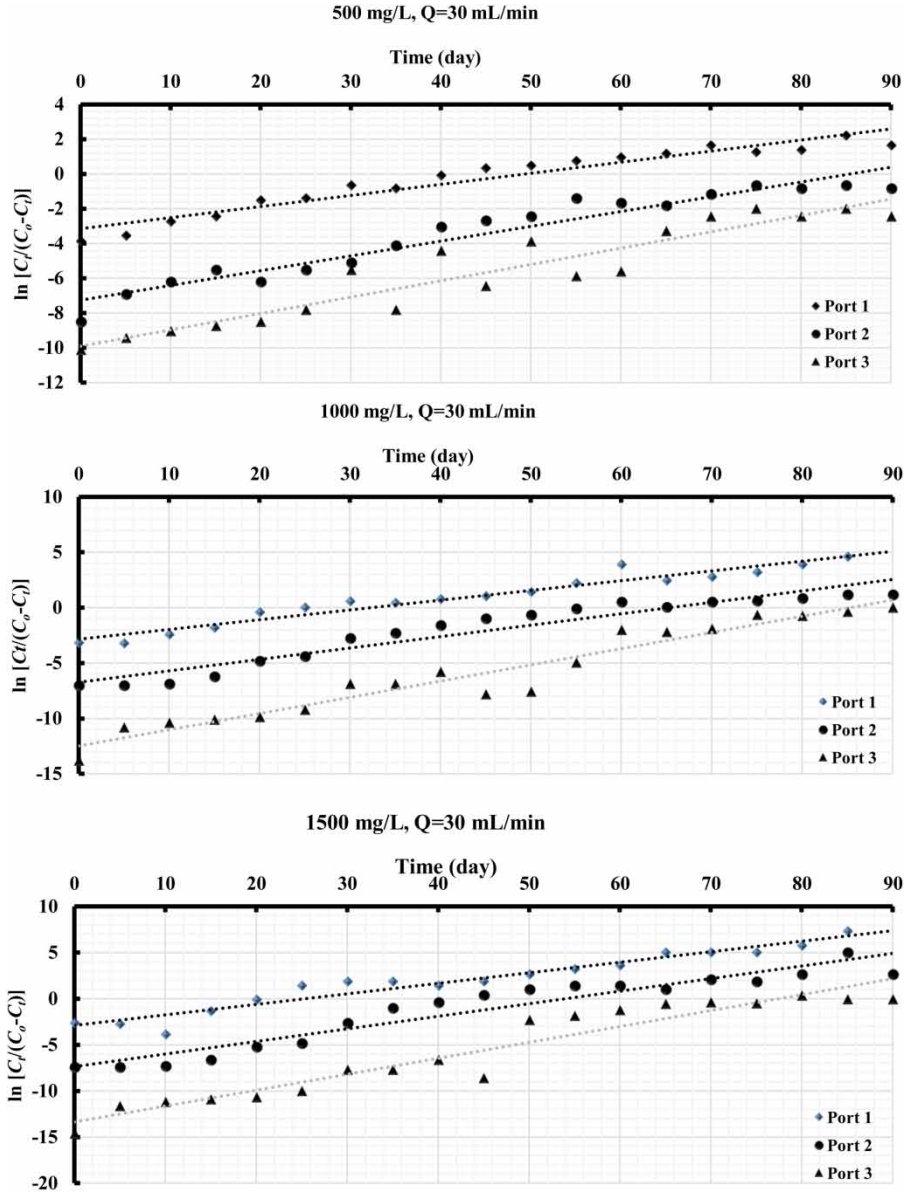


**Figure 6** | Yoon–Nelson model of breakthrough curves for CR with 30 mL/min flow rate and different initial concentration on adsorption.

coefficient decreased and the transport was slower, which gives a higher treated volume and a delayed adsorbent. Therefore, high effluent volume can be treated, as the solution stays in the bed for a long time, which increases with the bed height, giving it enough time to diffuse to the sorbent.

The COMSOL, Yoon–Nelson, Thomas, and Clark models can be applied to present the theoretical verification for the bed experiment by using the sorbent-filter glass waste as PRB. The values of $K_{\mathrm{YN}}$ were decreased and the values of $\tau$ were increased as the bed heights increased; also the Yoon–Nelson model at a higher inflow concentration was an effective simulation of the whole adsorbent. The value of $q_o$ increased when the concentration of the CR dye and the height of the bed (adsorbent mass) both increased, the value of the Thomas rate constant ($K_{Th}$) increased, and the value of $q_o$ decreased. The CR dye adsorption increased when the adsorbent bed depth was higher and when the initial concentration of CR dye was lower. The Yoon–Nelson and Thomas models were good at simulating the adsorption process, and the Clark model had a low described

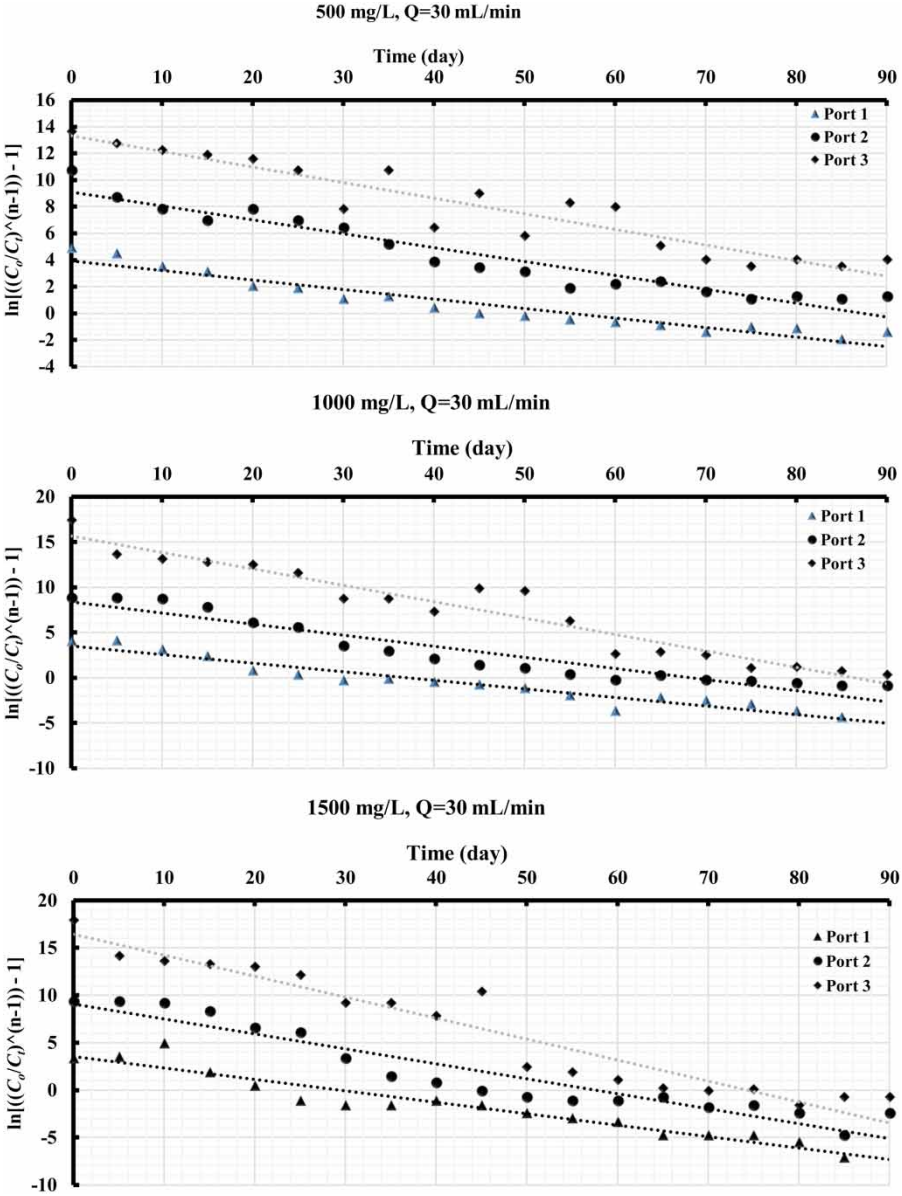


**Figure 7** | Clark model of breakthrough curves for CR with 30 mL/min flow rate and different initial concentration on adsorption.

adsorption breakthrough, but the COMSOL model was the best simulation of the adsorption breakthrough, with higher $R^2 = 0.96$.

## ACKNOWLEDGEMENTS

We would like to gratefully acknowledge the technical support of Laith A. Naji, Technical Instructors Training Institute, Middle Technical University and Kerbala University, Civil Engineering department.

## DATA AVAILABILITY STATEMENT

All relevant data are included in the paper or its Supplementary Information.

## REFERENCES

Abd Ali, Z. T., Naji, L. A., Almuktar, S. A. A. A. N., Faisal, A. A. H., Abed, S. N., Scholz, M., Naushad, M. & Ahamad, T. 2020 Predominant mechanisms for the removal of nickel

metal ion from aqueous solution using cement kiln dust. *Journal of Water Process Engineering* **33**, 101033. https://www.sciencedirect.com/science/article/pii/S2214714419312371.

Ahmed, D. N., Naji, L. A., Faisal, A. A. H., Al-Ansari, N. & Naushad, M. 2020 Waste foundry sand/MgFe-layered double hydroxides composite material for efficient removal of Congo Red dye from aqueous solution. *Scientific Reports* **10**, 2042. https://www.nature.com/articles/s41598-020-58866-y.

Aksu, Z. & Gönen, F. 2004 Biosorption of phenol by immobilized activated sludge in a continuous packed bed: prediction of breakthrough curves. *Process Biochemistry* **39**, 599–613.

Al-Degs, Y. S., Khraisheh, M. A. M., Allen, S. J. & Ahmad, M. N. 2009 Adsorption characteristics of reactive dyes in columns of activated carbon. *Journal of Hazardous Materials* **165**, 944–949.

Alshammari, M., Al Juboury, M. F., Naji, L. A., Faisal, A. A. H., Zhu, H., Al-Ansari, N. & Naushad, M. 2020 Synthesis of a novel composite sorbent coated with siderite nanoparticles and its application for remediation of water contaminated with Congo Red dye. *International Journal of Environmental Research* **14**, 177–191.

Amaniampong, P. N., Trinh, Q. T., Wang, B., Borgna, A., Yang, Y. & Mushrif, S. H. 2015 Biomass oxidation: formyl C–H bond activation by the surface lattice oxygen of regenerative CuO nanoleaves. *Angewandte Chemie.* **54**, 8928–8933.

Amaniampong, P. N., Trinh, Q. T., Varghese, J. J., Behling, R., Valange, S., Mushrif, S. H. & Jérôme, F. 2018 Unraveling the mechanism of the oxidation of glycerol to dicarboxylic acids over a sonochemically synthesized copper oxide catalyst. *Green Chemistry* **20**, 2730–2741.

Ambrosini, G. S. D. 2004 *Reactive Materials for Subsurface Remediation Through Permeable Reactive Barriers*. PhD thesis, Swiss Federal Institute of Technology, Zurich, Switzerland. https://doi.org/10.3929/ethz-a-004938965.

Baral, S. S., Das, N., Ramulu, T. S., Sahoo, S. K., Das, S. N. & Chaudhury, G. R. 2009 Removal of Cr(VI) by thermally activated weed *Salvinia cucullata* in a fixed-bed column. *Journal of Hazardous Materials* **161**, 1427–1435.

Basibuyuk, M. & Kalat, D. G. 2004 The use of waterworks sludge for the treatment of vegetable oil refinery industry wastewater. *Environmental Technology* **25**, 373–380.

Bharathi, K. S. & Ramesh, S. P. T. 2013 Fixed-bed column studies on biosorption of crystal violet from aqueous solution by *Citrullus lanatus* rind and *Cyperus rotundus*. *Applied Water Science* **3**, 673–687.

Buasri, A., Yongbut, P., Chaiyut, N. & Phattarasirichot, K. 2008 Adsorption equilibrium of zinc ions from aqueous solution by using modified clinoptilolite. *Chiang Mai J. Sci.* **35**, 56–62.

Ciardelli, G., Corsi, L. & Marcucci, M. 2001 Membrane separation for wastewater reuse in the textile industry. *Resources, Conservation and Recycling* **31**, 189–197.

Clark, R. M. 1987 Evaluating the cost and performance of field-scale granular activated carbon systems. *Environmental Science and Technology* **21**, 573–580.

Djelloul, C. & Hamdaoui, O. 2014 Dynamic adsorption of Methylene Blue by melon peel in fixed-bed columns. *Desalination and Water Treatment* **56**, 1–10.

Doke, K. M., Yusufi, M., Joseph, R. D. & Khan, E. M. 2012 Biosorption of hexavalent chromium onto wood apple shell: equilibrium, kinetic and thermodynamic studies. *Desalination and Water Treatment* **50**, 170–179.

Faisal, A. A. H. & Naji, L. A. 2019 Simulation of ammonia nitrogen removal from simulated wastewater by sorption onto waste foundry sand using artificial neural network. *Association of Arab Universities Journal of Engineering Sciences* **26**, 28–34.

Faisal, A. A. H., Al-Wakel, S. F. A., Assi, H. A., Naji, L. A. & Naushad, M. 2020a Waterworks sludge-filter sand permeable reactive barrier for removal of toxic lead ions from contaminated groundwater. *Journal of Water Process Engineering* **33**, 101112. https://www.sciencedirect.com/science/article/pii/S2214714419316988.

Faisal, A. A. H., Alquzweeni, S. S., Naji, L. A. & Naushad, M. 2020b Predominant mechanisms in the treatment of wastewater due to interaction of benzaldehyde and iron slag by product. *International Journal of Environmental Research and Public Health* **17**, 226. https://www.mdpi.com/1660-4601/17/1/226.

Faisal, A. A. H., Ibreesam, M. M., Al-Ansari, N., Naji, L. A., Naushad, M. & Ahamad, T. 2020c COMSOL multiphysics 3.5a package for simulating the cadmium transport in the sand bed-bentonite low permeable barrier. *Journal of King Saud University – Science* **32**, 1944–1952.

Faisal, A. A. H., Nassir, Z. S., Naji, L. A., Naushad, M. & Ahamad, T. 2020d A sustainable approach to utilize olive pips for the sorption of lead ions: numerical modeling with aid of artificial neural network. *Sustainable Chemistry and Pharmacy* **15**. https://www.sciencedirect.com/science/article/pii/S2352554119303043.

Goel, J., Kadirvelu, K., Rajagopal, C. & Kumar, G. V. 2005 Removal of lead(II) by adsorption using treated granular activated carbon: batch and column studies. *Journal of Hazardous Materials* **125**, 211–220.

Hadi, M., Samarghandi, M. R. & McKay, G. 2011 Simplified fixed bed design models for the adsorption of acid dyes on novel pine cone derived activated carbon. *Water, Air, and Soil Pollution* **218**, 1–4.

Hamdaoui, O. 2006 Dynamic sorption of Methylene Blue by cedar sawdust and crushed brick in fixed bed columns. *Journal of Hazardous Materials* **138**, 293–303.

Han, R., Wang, Y., Yu, W., Zou, W., Shij, J. & Liu, H. 2007 Biosorption of Methylene Blue from aqueous solution by rice husk in a fixed-bed column. *Journal of Hazardous Materials* **141**, 713–718.

Hashim, M. A., Mukhopadhyay, S., Sahu, J. N. & Sengupta, B. 2011 Remediation technologies for heavy metal contaminated groundwater. *Journal of Environmental Management* **92**, 2355–2388.

Ho, Y. S. & McKay, G. 1999 Pseudo-second order model for sorption processes. *Process Biochemistry* **34**, 451–465.

Hu, W., Lu, S., Song, W., Chen, T., Hayat, T., Alsaedi, N. S., Chen, C. & Liu, H. 2018 Competitive adsorption of U(VI) and Co(II) on montmorillonite: a batch and spectroscopic approach. *Applied Clay Science* **157**, 121–129. https://doi.org/10.1016/j.clay.2018.02.030.

ITRC 2011 *Permeable reactive barriers: lessons learned/new directions* 2011 (PRB-4) Feb-05, Interstate Technology & Regulatory Council, Permeable Reactive Barriers Team, Washington, DC.

Jin, X., Zha, S., Li, S. & Chen, Z. 2014 Simultaneous removal of mixed contaminants by organoclays – amoxicillin and Cu(II) from aqueous solution. *Applied Clay Science* **102**, 196–201.

Lagergren, S. 1989 About the theory of so-called adsorption of soluble substances. *Kung Seventeen Hand* **24**, 1–39.

Li, W., Yue, Q., Tu, P., Ma, Z., Gao, B., Li, J. & Xu, X. 2011 Adsorption characteristics of dyes in columns of activated carbon prepared from paper mill sewage sludge. *Chemical Engineering Journal* **178**, 197–203.

Limousin, G., Gaudet, J.-P., Charlet, L., Szenknect, S., Barthès, V. & Krimissa, M. 2007 Sorption isotherms: a review on physical bases, modeling and measurement. *Applied Geochemistry* **22**, 249–275.

Markovska, L., Meshko, V. & Noveski, V. 2001 Adsorption of basic dyes in a fixed bed column. *Korean Journal of Chemical Engineering* **18**, 190–195.

Mathews, A. P. & Zayas, I. 1989 Particle size and shape effects on adsorption rate parameters. *Journal of Environmental Engineering* **115**, 41–55.

Mishra, A. K., Ohtsubo, M., Li, L. & Higashi, T. 2011 Controlling factors of the swelling of various bentonites and their correlations with the hydraulic conductivity of soil-bentonite mixtures. *Applied Clay Science* **52**, 78–84.

Miz, M. E., Akichouh, H., Salhi, S., Bachiri, A. E. & Tahani, A. 2014 Adsorption–desorption and kinetics studies of Methylene Blue dye on Na–bentonite from aqueous solution. *IOSR Journal of Applied Chemistry* **7**, 60–78.

Mobasherpour, I., Salahi, E. & Asjodi, A. 2014 Research on the batch and fixed-bed column performance of red mud adsorbents for lead removal. *Canadian Chemical Transactions* **4**, 83–96.

Naji, L. A., Jassam, S. H., Yaseen, M. J., Faisal, A. A. H. & Al-Ansari, N. 2019 Modification of Langmuir model for simulating initial pH and temperature effects on sorption process. *Separation Science and Technology* **55** (15), 2729–2736. https://www.tandfonline.com/doi/full/10.1080/01496395.2019.1655055.

Naji, L. A., Faisal, A. A. H., Rashid, H. M., Naushad, M. & Ahamad, T. 2020 Environmental remediation of synthetic leachate produced from sanitary landfills using low-cost composite sorbent. *Environmental Technology & Innovation* **175**, 100680. https://www.sciencedirect.com/science/article/abs/pii/S2352186420300286.

Ott, N. 2000 *Permeable Reactive Barriers for Inorganics*. Report U.S. Environmental Protection Agency Office of Solid Waste and Emergency Response Technology Innovation Office, Washington, DC.

Padmesh, T. V. N., Vijayaraghavan, K., Sekaran, G. & Velan, M. 2005 Batch and column studies on biosorption of acid dyes on fresh water macro alga *Azolla filiculoides*. *Journal of Hazardous Materials* **125**, 121–129.

Paul, R., Sarkar, C., Yan, Y., Trinh, Q. T., Rao, B. S., Pao, C., Lee, J., Liu, W. & Mondal, J. 2020 Porous-organic-polymer-triggered advancement of sustainable magnetic efficient catalyst for chemoselective hydrogenation of cinnamaldehyde. *ChemCatChem* **12**, 3687–3704. https://doi.org/10.1002/cctc.202000072.

Phuengprasop, T., Sittiwong, J. & Unob, F. 2011 Removal of heavy metal ions by iron oxide coated sewage sludge. *Journal of Hazardous Materials* **186**, 502–507.

Rahi, M. A., Faisal, A. A. H., Naji, L. A., Almuktar, S. A., Abed, S. N. & Scholz, M. 2020 Biochemical performance modelling of non-vegetated and vegetated vertical subsurface-flow constructed wetlands treating municipal wastewater in hot and dry climate. *Journal of Water Process Engineering* **33**, 101003. https://www.sciencedirect.com/science/article/pii/S2214714419309079.

Saad, N., Abd, A. Z. T., Naji, L. A., Faisal, A. A. A. H. & Al-Ansari, N. 2019 Development of Bi-Langmuir model on the sorption of cadmium onto waste foundry sand: effects of initial pH and temperature. *Environmental Engineering Research* **25**, 677–684.

Sadaf, S. & Bhatti, H. N. 2014 Evaluation of peanut husk as a novel, low cost biosorbent for the removal of Indosol Orange RSN dye from aqueous solutions: batch and fixed bed studies. *Clean Technologies and Environmental Policy* **16**, 527–544.

Saha, P. D., Chowdhury, S., Mondal, M. & Sinha, K. 2012 Biosorption of direct Red 28 (Congo Red) from aqueous solutions by eggshells: batch and column studies. *Separation Science and Technology* **47**, 112–123.

Sahoo, J. K., Paikra, S. K., Mishra, M. & Sahoo, H. 2019 Amine functionalized magnetic iron oxide nanoparticles: synthesis, antibacterial activity and rapid removal of Congo Red dye. *Journal of Molecular Liquids* **282**, 428–440.

Sarkar, C., Pendem, S., Shrotri, A., Dao, D. Q., Pham Thi Mai, P., Nguyen Ngoc, T., Chandaka, D. R., Rao, T. V., Trinh, Q. T., Sherburne, M. P. & Mondal, J. 2019 Interface engineering of graphene-supported Cu nanoparticles encapsulated by mesoporous silica for size-dependent catalytic oxidative coupling of aromatic amines. *ACS Applied Materials & Interfaces* **11**, 11722–11735. https://doi.org/10.1021/acsami.8b18675.

Sarkar, C., Shit, S. C., Dao, D. Q., Lee, J., Tran, N. H., Singuru, R., An, K., Nguyen, D. N., Van, L. Q., Amaniampong, P. N., Drif, A., Jerome, F., Huyen, P. T., Phan, T. T. N., Vo, D.-V. N., Thanh Binh, N., Trinh, Q. T., Sherburne, M. P. & Mondal, J. 2020 An efficient hydrogenation catalytic model hosted in a stable hyper-crosslinked porous-organic-polymer: from fatty acid to bio-based alkane diesel synthesis. *Green Chemistry* **22**, 2049–2068. https://doi.org/10.1039/C9GC03803E.

Sepehr, M. N., Amrane, A., Karimaian, K. A., Zarrabi, M. & Ghaffari, H. R. 2014 Potential of waste pumice and surface modified pumice for hexavalent chromium removal: characterization, *equilibrium, thermodynamic and kinetic*

*study*. *Journal of the Taiwan Institute of Chemical Engineers* **45**, 635–647.

Shetti, N. P., Malode, S. J., Malladi, R. S., Nargund, S. L., Shukla, S. S. & Aminabhavi, T. M. 2019 Electrochemical detection and degradation of textile dye Congo Red at graphene oxide modified electrode. *Microchemical Journal* **146**, 387–392.

Simantiraki, F., Kollias, C. G., Maratos, D., Hahladakis, J. & Gidarakos, E. 2013 Qualitative determination and application of sewage sludge and municipal solid waste compost for BTEX removal from groundwater. *Journal of Environmental Chemical Engineering* **1**, 9–17.

Simon, F. G. & Meggyes, T. 2002 Removal of organic and inorganic pollutants from groundwater using permeable reactive barriers: part 1–treatment processes for pollutants. *Land Contamination and Reclamation* **8** (2), 103–116.

Singuru, R., Trinh, Q. T., Banerjee, B., Govinda Rao, B., Bai, L., Bhaumik, A., Reddy, B. M., Hirao, H. & Mondal, J. 2016 Integrated experimental and theoretical study of shape-Controlled catalytic oxidative coupling of aromatic amines over CuO nanostructures. *ACS Omega* **1**, 1121–1138. https://doi.org/10.1021/acsomega.6b00331.

Somasekhara, R. M. C. & Nirmala, V. 2019 Bengal gram seed husk as an adsorbent for the removal of dyes from aqueous solutions – column studies. *Arabian Journal of Chemistry* **12**, 1695–1706.

Sulaymon, A. H., Faisal, A. A. H. & Khaliefa, Q. M. 2015 Cement kiln dust (CKD)-filter sand permeable reactive barrier for the removal of Cu(II) and Zn(II) from simulated acidic groundwater. *Journal of Hazardous Materials* **297**, 160–172.

Thomas, W. J. & Crittenden, B. 1998 *Adsorption Technology and Design*. Oxford, Butterworth-Heinemann. https://doi.org/10.1016/B978-075061959-2/50002-1.

Wantanaphong, J., Mooney, S. J. & Bailey, E. H. 2005 Natural and waste materials as metal sorbents in permeable reactive barriers (PRBs). *Environmental Chemistry Letters* **3**, 19–23.

Yagub, M. T., Sen, T. K., Afroze, S. & Ang, H. M. 2015 Fixed-bed dynamic column adsorption study of Methylene Blue (MB) onto pine cone. *Desalination and Water Treatment* **55**, 1026–1039.

First received 28 June 2020; accepted in revised form 3 October 2020. Available online 16 October 2020